



Influence of Thermal Treatment on Crystallization and Course of Martensitic Transformation in Ni₂₅Ti₅₀Cu₂₅ Alloys Produced via High-Energy Ball Milling

Tomasz Goryczka¹ · Grzegorz Dercz¹

Received: 26 January 2023 / Revised: 12 April 2023 / Accepted: 24 April 2023 / Published online: 30 May 2023
© The Author(s) 2023, corrected publication 2023

Abstract The alloy with the chemical composition of Ni₂₅Ti₅₀Cu₂₅ and a weight of 20 g was produced via high-energy ball milling that lasted 100 h, 120 h, and 140 h. After grinding, the powders consisted of an amorphous-nanocrystalline mixture formed from solid solutions based on alloying elements and a phase being a precursor of the intermetallic β phase. This phase undergoes the reversible martensitic transformation in NiTiCu alloys. Crystallization occurred in several stages, ranging from 361 to 556 °C. Using short-term annealing followed by the X-ray quantitative analysis, the crystallized phases sequence and their weight percentages were determined after each stage. Annealing of the crystallized alloy lasted from 5 min to 20 h in the temperature ranges from 700 to 1000 °C, which revealed the quantitative evolution of the equilibrium phases and the martensitic transformation evolution. Moreover, following thermal treatment steps, the transformation changed from the B2 ↔ B19' to the B2 ↔ B19, as expected for the Ni₂₅Ti₅₀Cu₂₅ alloy.

Keywords Martensitic transformation · NiTiCu · Heat treatment · High-energy ball milling

Introduction

Ternary alloys based on NiTi with the addition of copper, instead of nickel, are in the application spotlight [1–3] due to the possibility of multistage martensitic transformation in the range from room temperature to about 100 °C [4]. Moreover, replacing half of the nickel content with copper, leads to a unique one-stage transformation with a characteristic narrow temperature hysteresis of several degrees. The multistage martensitic transformation in NiTi alloys can be achieved by adding such alloying elements as Fe, Ag, Cr, and Co. However, the MT temperature range is below 50 °C and most of all in subzero temperatures [5].

The properties of shape memory alloys and the associated occurrence of the reversible martensitic transformation also depend on the manufacturing method. Many techniques used in metallurgy, which can control the martensitic transformation parameters, have been adopted to produce shape memory alloys (SMA). The basic ones are classical casting and obtaining NiTi-based alloys in the form of bulk [6–9]. The use of rapid solidification allows for producing SMAs as layers, tapes, or strips in the amorphous, nanocrystalline, or fully crystallized state [10–13]. On the other hand, the additive manufacturing methods result in the macro scale production in any programmable shape [9, 14]. Also, the methods based on severe plastic deformation supported by appropriate heat treatment make it possible to obtain an alloy from an amorphous to crystalline state [15–18]. However, it is a bulk material. For the production of NiTi-based alloys in the form of powders with nanometric average grain size, the alloy atomization is used [19, 20]. Still, mechanical alloying remains the only method to produce powders with an average grain size measured in micrometers.

This article is an invited submission to *Shape Memory and Superelasticity* selected from presentations at the 12th European Symposium on Martensitic Transformations (ESOMAT 2022) held September 5–9, 2022 at Hacettepe University, Beytepe Campus, Ankara, Turkey, and has been expanded from the original presentation. The issue was organized by Prof. Dr. Benat Koçkar, Hacettepe University.

✉ Tomasz Goryczka
tomasz.goryczka@us.edu.pl

¹ Institute of Materials Engineering, University of Silesia in Katowice, 75 Pułku Piechoty 1A, 41-500 Chorzow, Poland

An example of mechanical alloying is high-energy milling which leads to the alloy amorphization. Primarily, such studies were carried out for the NiTi alloy. The results showed that the high milling speed (to 700 rpm) led to an alloy with a low weight of about 10 g in the amorphous-nanocrystalline form [21–24]. In our previous work the Ni₂₅Ti₅₀Cu₂₅ alloy was obtained as a micrometric powder [24, 25]. However, the batch mass was 10 g resulting in an amorphous-nanocrystalline mixture. Apart from the batch material, the limitation in the alloy's production is the container's capacity which can hold an appropriate number/volume of balls. Therefore, our work aimed to obtain the Ni₂₅Ti₅₀Cu₂₅ alloy with twice the weight of the charge, maintaining the same balls to the grinding material ratio and the low grinding speed. This assumption impacted the alloy components, their crystallization, and the final chemical and phase composition formation. Our studies showed the evolution of the Ni₂₅Ti₅₀Cu₂₅ alloy formation in a powder form, depending on the applied heat treatment, from crystallization to the expected final homogenization. Moreover, at all the stages, the course of the reversible martensitic transformation was investigated.

Materials and Methods

Commercially available powders of the alloying elements: nickel, titanium, and copper of technical purity were used to produce an alloy with a chemical composition of Ti: 50 at.% and 25 at.% for Ni and Cu, respectively. The nickel and copper particles were spherical, with an average grain size of 11 μm and 6 μm . In contrast, the titanium particles, with an average size of 34 μm , were irregular (Fig. 1). The samples of 20 g were processed in the high-energy Fritsch Pulverisette 7 premium line planetary-ball mill (HEBM) using a relatively low speed of 250 rpm. It has been known that a relatively high milling speed (e.g., 350 or 700 rpm) increases the temperature in the container. Despite grinding in a protective atmosphere of argon, the elevated temperature causes the oxidation of the titanium powder surface, which might limit the diffusion of alloying elements. Therefore, in order to reduce the milling speed, the grinding time was extended to 100, 120, and 140 h. For milling to be effective, the powder weight to the balls weight ratio was 10:1. The heat treatment, in the range from room temperature (RT) to 600 °C, was carried out *in-situ* in a differential scanning calorimeter (DSC). Due to the limited operating range of the DSC (to 640 °C), the heat treatments at temperatures above 600 °C (from 700 to 1000 °C—every 100 degrees) were performed in a vacuum furnace (10^{-5} Pa) for the powder in the as-milled state.

The microstructure was observed using the JEOL JSM-6480 scanning electron microscope (SEM) equipped with

an energy-dispersive X-ray spectroscopy detector (EDS). The accelerating voltage was 20 kV. The observations were carried out on powders at various milling stages and on their metallographic cross-sections. The cross-sections were prepared from powders incorporated in graphite. The samples were automatically polished to the gradation of 1 μm , using abrasive papers and polishing suspensions.

The crystallization process and the martensitic transformation (MT) course were studied using differential scanning calorimetry (DSC). For this purpose, the Mettler Toledo DSC 1 calorimeter was used, operating in the temperature range from -140 to 650 °C in a protective argon atmosphere. In the case of overlapping thermal peaks, the DSC curves were deconvoluted using the Pearson IV function [26], obtaining χ^2 values of 0.99. The baseline was determined using instrument calibration with an indium standard. The starts and ends of the transformation temperature were determined from the intersection point of the tangent to the peak side and the baseline.

In order to determine the course of the crystallization process, the samples were heated at a rate of 20 deg/min. up to 600 °C by recording thermograms. Contrary to the alloy weighing 10 g which was milled for 100 h [23], the crystallization of the studied powders occurred in several stages. To study the multi-stage crystallization process, the samples were heated in the calorimeter to the temperature specified in Table 1 as T_{T1} , T_{T2} , and T_{T3} , stabilized for 30 s, and cooled down to -120 °C at the maximum rate. Then, in the range from -120 to 120 °C, the thermograms were measured at a rate of 10 deg/min. Due to the heating limit of the DSC (640 °C) and the fact that the alloy crystallized below 600 °C, the thermal treatment at the 700–1000 °C (every 100 degrees) range was done in a vacuum furnace (10^{-5} Pa).

The effect of the heat treatment on the alloy's formation and its phase composition evolution was studied using the X'Pert-PRO diffractometer (Malvern Panalytical Ltd., Malvern, UK). The Cu_{K α 1and2} radiation was applied. The diffractograms were measured at room temperature, in the angular range of 2θ from 10° to 140° using the step-scan method with a step of 0.03° or 0.04° and a time period adjusted to obtain the appropriate counting statistics. The phase identification was performed using the International Center for Diffraction Data (ICDD) PDF-4 + database. The Rietveld method [27] was applied to calculate the volume shares of the alloy's components. The crystallographic data for the construction of the phase models were provided by the ICDD base and the calculations were performed using the LHPM computer program (version 4.2. Lucas Heights Research Laboratories ANSTO, Sydney, Australia).

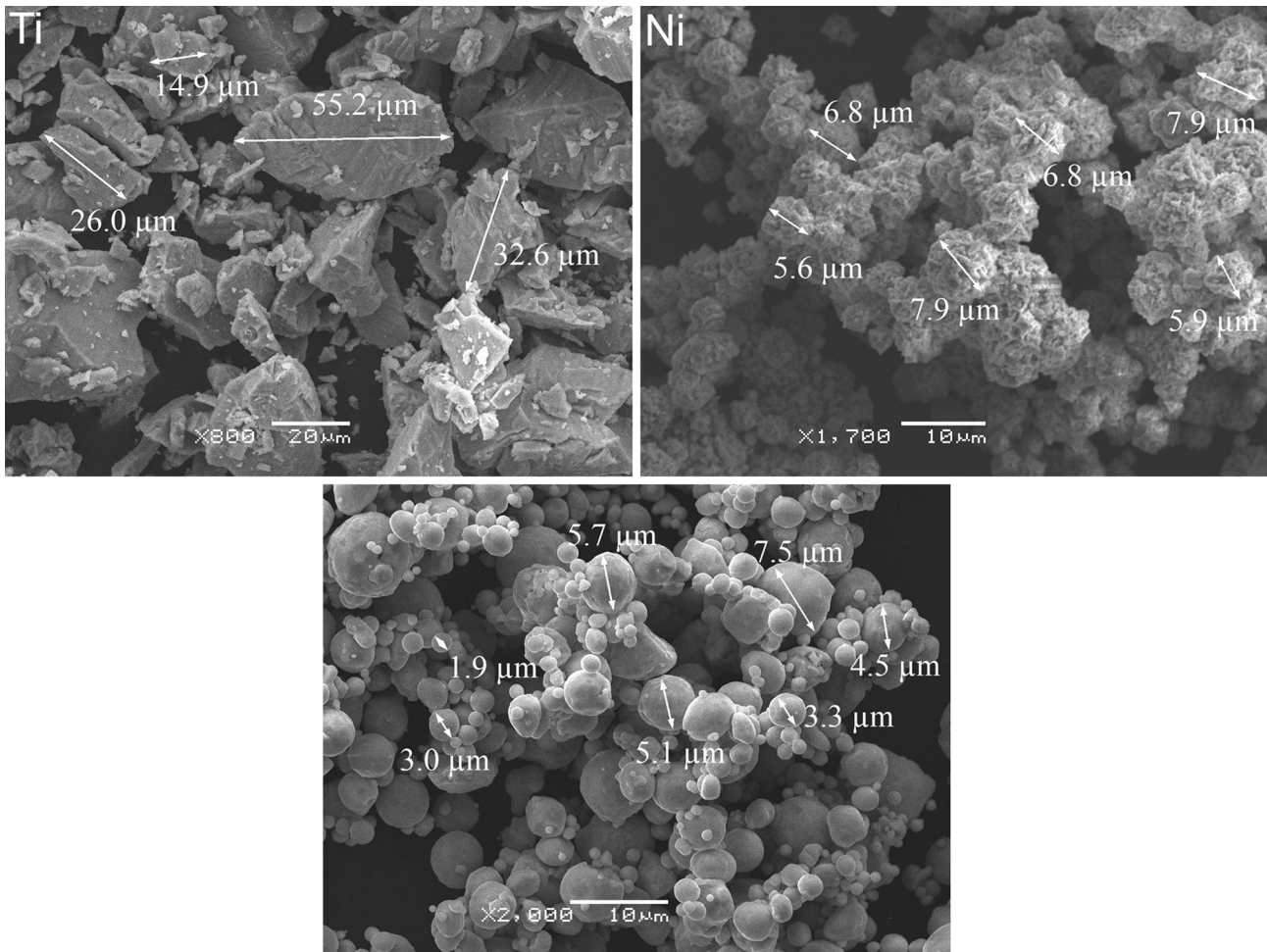


Fig. 1 SEM images observed for powders of the alloying elements

Table 1 Annealing temperatures for milled samples

Milling time [h]	Annealing temperature [°C]		
	T_{T1}	T_{T2}	T_{T3}
100	420	500	600
120	420	480	600
140	420	480	600

Results and Discussion

The heat treatment influence on the course of the martensitic transformation was analyzed in two aspects. The first one concerned the MT's course in the range of crystallization temperatures and its fragmentarily crystallized components. The other one focused on the influence of the crystallized alloy's annealing temperature on the MT's course.

Multistage Crystallization Process and Its Influence on Martensitic Transformation

As research shows, the charge weight is an important factor, despite maintaining the same ratio of the charge weight to the grinding balls weight and the same container's volume [24]. A ten-gram charge after 100 h of milling showed a completely amorphous-nanocrystalline form. In addition, the crystallization took place as a one-stage process. Doubling the weight of the charge caused its multi-stage course. The crystallization of the $Ni_{25}Ti_{50}Cu_{25}$ alloy was carried out in three stages. The measured thermograms for 100, 120, and 140 h of milled powders were compared in Fig. 2. The temperatures characterizing crystallization and enthalpy were determined from the thermograms and compared in Fig. 3. The summarized data in Fig. 2 show that crystallization occurred in three stages depending on the grinding time. It is evidenced by three peaks marked in Fig. 2 as Peak 1 (the red line), Peak 2 (the blue line), and Peak 3 (the green line). The peak

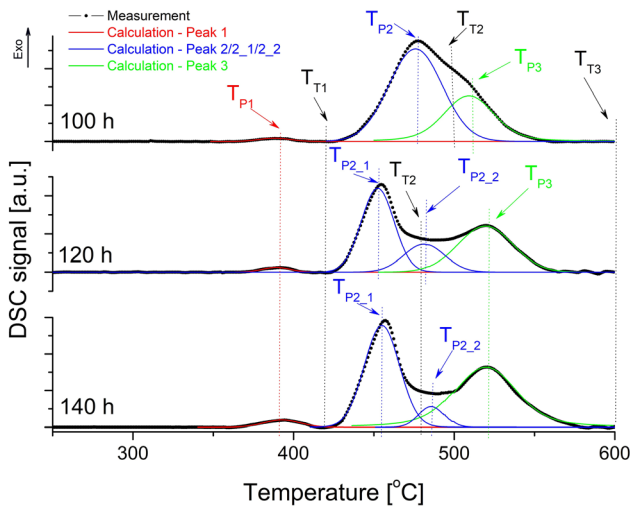


Fig. 2 Results of the thermal peak refinement done for the thermograms measured for 100, 120, and 140 h milled powders

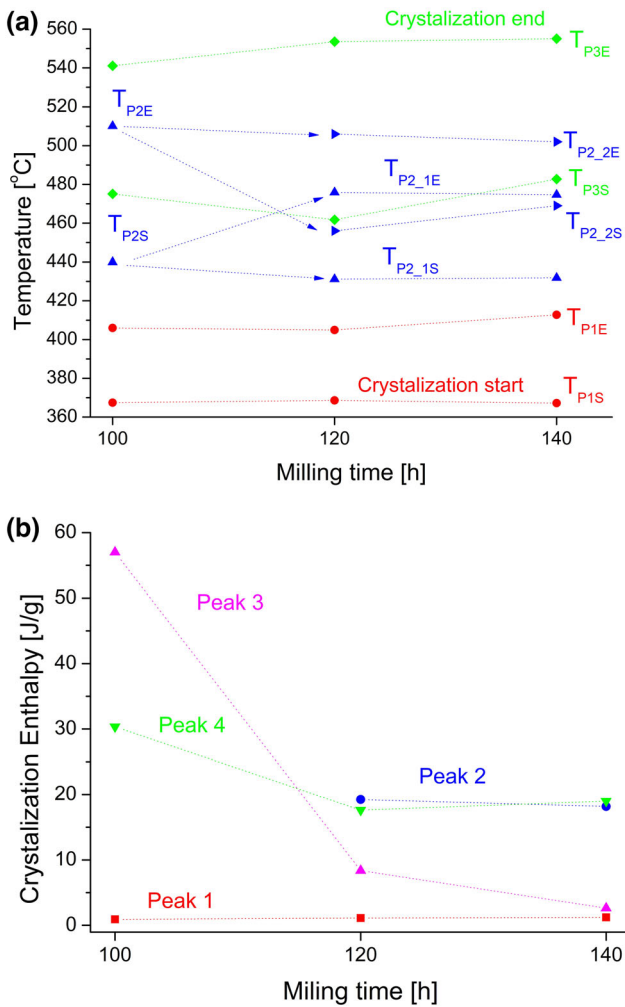


Fig. 3 Dependence of MT's characteristic temperatures (a) and crystallization enthalpy (b) on milling time

temperatures were marked as T_{P1} , T_{P2} (100 h) and T_{P2_1} , T_{P2_2} for 120 h and 140 h, and T_{P3} , respectively. Prolonging the grinding time to 120 h and 140 h separated the superimposed thermal Peaks 2 and 3 for 100 h. Another effect was splitting stage 2 (Peak 2—the blue line) into two components, related to the temperatures: T_{P2_1} and T_{P2_2} (Figs. 2, 3a, b). Stage 3 (Peak 3—the green line in Fig. 2) partially overlapped stage 2 for the 100 h milled sample, while the milling times of 120 h and 140 h shifted the crystallization toward higher temperatures. The first stage (Peak 1—the red line in Fig. 2) was separated from the others (Peak 2—the blue line and Peak 3—the green line) and occurred in the temperature range from 368 to 405 °C (100 h and 120 h) and up to 413 °C for the 140 h milled sample. The T_{1S} start temperature of the transformation was also the start temperature of the crystallization process. For all the milling times, T_{1S} showed the same value of 368 °C (Fig. 3a). Moreover, this stage was associated with the process consuming the lowest enthalpy, namely 0.9 J/g (100 h), 1.1 J/g (120 h), and 1.3 J/g (140 h) (Fig. 3b).

The second stage (Peak 2—the blue line in Fig. 2), for the sample milled for 100 h, started at 440 °C and ended at 510 °C (Fig. 3a— T_{P2S} , T_{P2E}). This stage for the grinding times of 120 h and 140 h split into two thermal peaks: Peak 2_1 and Peak 2_2 (Figs. 2, 3a, b). For the milling time of 120 h, the start temperature of the first one (T_{P2_1S}) was 431 °C, while the end temperature (T_{P2_1E}) was 475 °C. The other component of the process started at T_{P2_2S} and equaled 456 °C, and ended at 481 °C (T_{P2_2E}). These temperatures were comparable to the ones determined for the milling time of 140 h. It follows that the temperature range of stage 2 for 100 h was almost identical to the sum of Peak 2_1 and Peak 2_2 determined for 120 h and 140 h. It is worth noting that the enthalpy change of processes associated with Peak 2 (100 h) was—57 J/g (Fig. 3b). This means that the process associated with this crystallization component released the highest energy, as compared to other components. For the milling time of 120 h, the enthalpy change of the 2_1 and 2_2 Peaks was – 19 J/g and – 8 J/g, respectively. For 140 h, it was – 18 J/g and – 3 J/g (Fig. 3b). The comparison of the enthalpies sum for the times of 120 h—27 J/g and 140 h – 21 J/g showed that the Peak 2 transformation released less energy as the grinding time increased.

The third stage of the crystallization process (Peak 3—the green line in Fig. 2) occurred in similar temperature ranges for all the milling times. It started at 475 °C (T_{P3S}) for the 100 h milled alloy, while for the 120 h and 140 h, it was about 14 degrees lower: 461 °C and 482 °C, respectively (Fig. 3a). The enthalpy change of this part of the crystallization process was – 30 J/g, – 18 J/g, and – 19 J/g for 100 h, 120 h, and 140 h, respectively (Fig. 3b).

The end temperature of the third stage (T_{P3E}) was also the end temperature of the crystallization process. Hence, the crystallization end temperature for the sample milled for 100 h was 541 °C and it increased to 554 °C, and to 555 °C for the samples milled for 120 h and 140 h, respectively (Fig. 3a). Compared to the single-stage crystallization described in [24], the crystallization start temperatures were lower by about 128°, whereas the ends were comparable.

To determine the sequence of the melt phases undergoing crystallization and their quantitative share, the milled powders were *in-situ* heated in the DSC to the temperatures characteristic for the individual stages of crystallization marked as T_{T1} , T_{T1} , and T_{T3} (Fig. 2 and Table 1), then stabilized and rapidly cooled. For such powders, the diffractograms and thermograms were measured. First, the phase identification was performed based on the X-ray diffraction patterns. Then the structural calculations were carried out using the Rietveld method. The ICDD crystallographic data of the unit cells were used to calculate the theoretical diffractograms. In the case of quantitative analysis, it was essential to obtain the best match between the measured and calculated diffraction patterns. The quality of the fit affected the error of the determined quantitative shares of individual phases. Therefore, to minimize the errors, the diffractograms were measured using the proper relation of the measurement step to the counting time, selected individually for the measured sample. The quality of the measured diffraction patterns was assessed on a reliability factor determining the accuracy of the statistical data of the measured diffraction patterns—the R_{exp} coefficient. Its value was ranging from 2.2 to 2.9%. The fitting was carried out until the coefficients R_p and R_{WP} were lower than 2.8 and 3.5%, respectively. In addition, the refinement quality was evaluated from the differential curve (the green line in Fig. 4), which showed the difference between the measured and calculated intensity. For the multiphase diffractograms, the obtained matches were of the highest quality. The exemplary results of the Rietveld analysis done for the 140 h milled sample, in the initial state and after the selected annealing temperatures, are shown in Fig. 4. The determined quantitative shares of individual phases are summarized in Fig. 5.

Having been milled, the powders consisted of an amorphous-nanocrystalline mixture (ANM) and solid solutions based on Ni, Cu, and Ti (Fig. 5a, c, e). The authors in [21, 28–30] reported that for NiTi and NiTiCu alloys (prepared by techniques leading to amorphization/nanocrystallization) the broadening of two peaks appearing in the X-ray diffraction patterns was associated with the presence of the amorphous phase. The results of our research and observations via high-resolution electron

microscopy HRTEM [25] showed that “the amorphous phase” was a mixture of an amorphous phase and nanocrystallites with an average size of 1.5–4 nm coming from various phases. Hence, in the description and discussion of the results, the name amorphous-nanocrystalline mixture (ANM) is used regarding this state of the ground material. Milling for 100 h was insufficient to obtain more than 40% of the ANM. The weight share for the titanium-based solid solution was about 53%, while the nickel-based and copper-based solid solutions were 2% and 5%, respectively. This fact indicated that the amorphous-nanocrystalline mixture mainly comprised nickel and copper elements, whereas titanium did not participate in its formation. According to the Ni-Cu phase equilibrium systems, both elements can form solid solutions in a whole range of concentrations [31]. On the other hand, titanium with nickel and copper forms solid solutions, but to a limited extent which tends to almost zero in the equilibrium conditions at room temperature, [32]. In relation to the equilibrium conditions, the solubility ranges are expected to increase in the manufacturing methods, such as high-energy ball milling or rapid solidification.

As the grinding time was increased to 120 h or 140 h, the proportion of the ANM mixture increased to 62% and 84%, respectively. In contrast, in the case of 140 h the proportions of Ni-, Cu-, and Ti-based solid solutions decreased to 1.7%, 0.5%, and 14%, respectively. This fact means that the diffusion of alloying elements took place in the amorphous-nanocrystalline mixture. Further, a matrix is formed from the intermetallic β phase with the chemical composition tending toward the nominal one.

The temperature raised to 420 °C (higher than T_{PIE}) changed the formation of crystalline alloy components. First of all, the energy supply significantly decreased the ANM mixture share. This process was intense in the powders milled for 100 h and 120 h, i.e., by 20% and 50%, respectively. In contrast, in the 140 h ground powder the ANM share was lowered to 4%. Hence, the shorter milling times (100 h and 120 h) resulted in less homogenous chemical composition. When higher internal stresses were introduced, the energy stored in structural defects lowered the crystallization temperature. This problem was discussed for the NiTi alloy in [24]. At the same time, raising the temperature to 420 °C caused the β phase formation that assumed the parent phase B2 structure at RT, regardless of the grinding time (Fig. 5b, d, f). The measured DSC cooling/heating curves in the – 120 °C to 120 °C range did not show any thermal peak in this area (Fig. 6—the black line). It follows that the high internal stresses coupled with the small sized crystallites suppressed the martensitic transformation [25]. In addition to the β phase crystallization, the weight percentage of the crystallized solid solutions decreased in the 100 h milled alloy. In contrast,

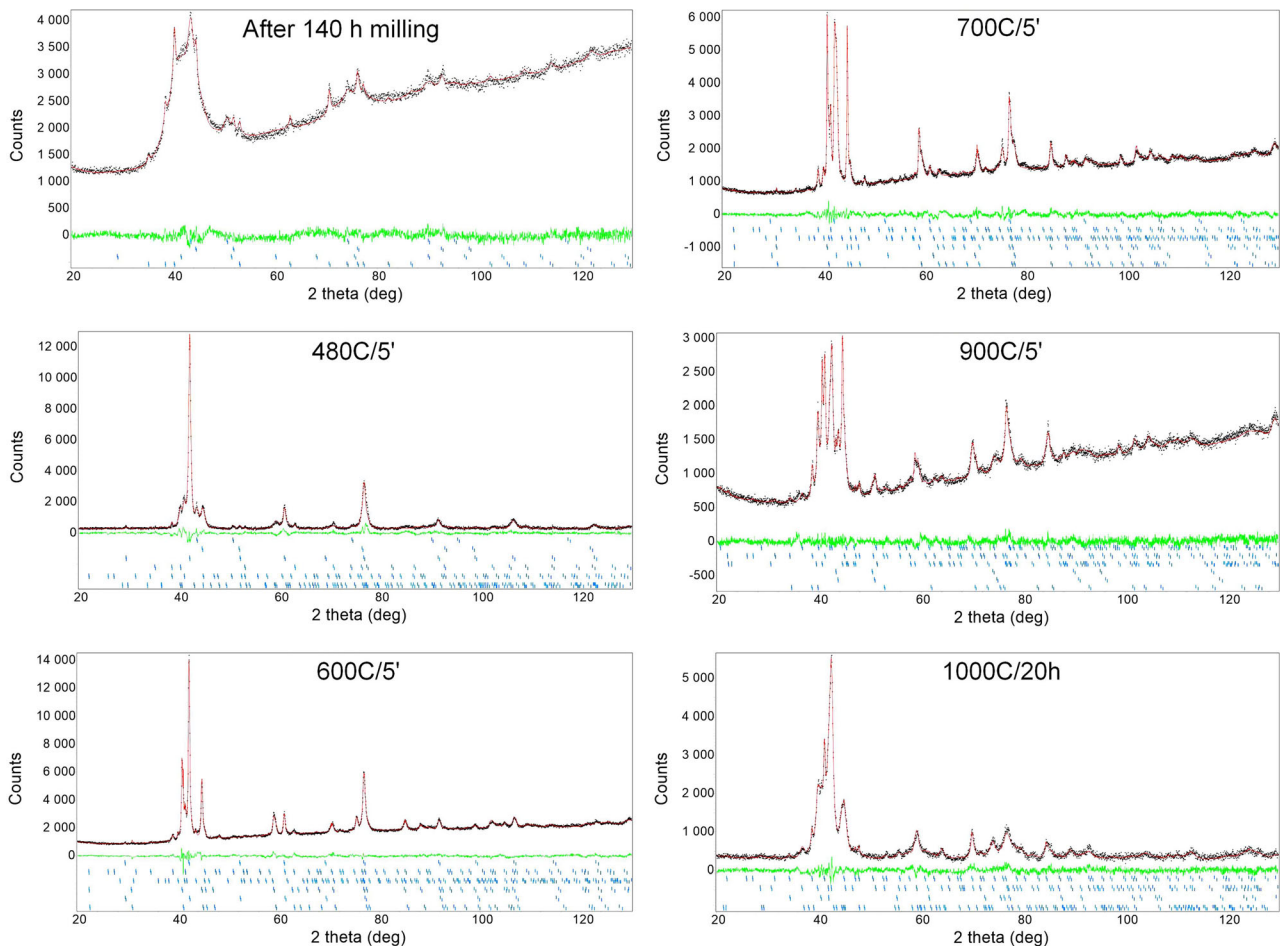


Fig. 4 Results of the Rietveld analysis obtained for the alloy ground 140 h and annealed at exemplary selected temperatures

after 120 h of grinding, the share of crystalline solid solutions based on titanium and copper increased. In contrary, the nickel-based solution share decreased, possibly due to the partial diffusion of nickel into the copper and titanium-based solution. In the 140 h milled powder the shares of all the three solutions diminished to trace amounts. On the other hand, the share of the Ti-based solid solution went down to about 4%, allowing the non-transformable $Ti_2(Ni,Cu)$ phase to be formed.

Increasing the temperatures to 500 °C in the 100 h milled alloys and to 480 °C the 120 h and 140 h ones significantly boosted the martensitically transformable β phase. This fact was related to reducing the ANM share to only a few percent. It means that Peak 2 (for 100 h) and Peak 2_1 (120 h and 140 h) were mainly related to the β phase crystallization. In this case, the β phase also adopted the B2-type structure, characteristic for the parent phase at room temperature. In addition, the formation of martensitically non-transformable $Ti_2(Ni,Cu)$ phases began. For the poorly homogenized 100 h milled powder, the tetragonal $Ti(Cu,Ni)_2$ phase appeared. Its formation is discussed in detail in chapter 3.2. Hence, Peak 2_2 occurring in the

DSC heating curves was associated with the $Ti_2(Ni,Cu)$ phase formation. Changing the fractions of crystalline phases caused by the elevated temperature (500 °C for 100 h of milling and 480 °C for 140 h) and the lowered internal stresses positively affected the reversible martensitic transformation. The measured thermograms showed the presence of one peak on the heating and cooling curves for all the milling times (Fig. 6). However, the range measured for the forward and reverse transformation was quite large. The difference between the beginning (M_s and M_f) and the end of the transformation (A_s and A_f) equaled almost 70 degrees (Fig. 7a) for the sample milled 100 h. In contrast, for 140 h it decreased to about 30 degrees (Fig. 7b). This effect resulted from the dispersed chemical composition affecting the characteristic temperatures of the martensitic transformation and the low content of copper in the β phase. As shown in [33], the low copper content (2–5at.%) exchanged for nickel in the $Ni_{(50-X)}Ti_{50}Cu_X$ alloy may reduce M_s even to -150 °C. Also, the low transformation enthalpy (1 J/g) indicated that a small amount of the phase underwent the MT, however, its weight share was relatively high: 50% (100 h) and almost 60% (140 h)

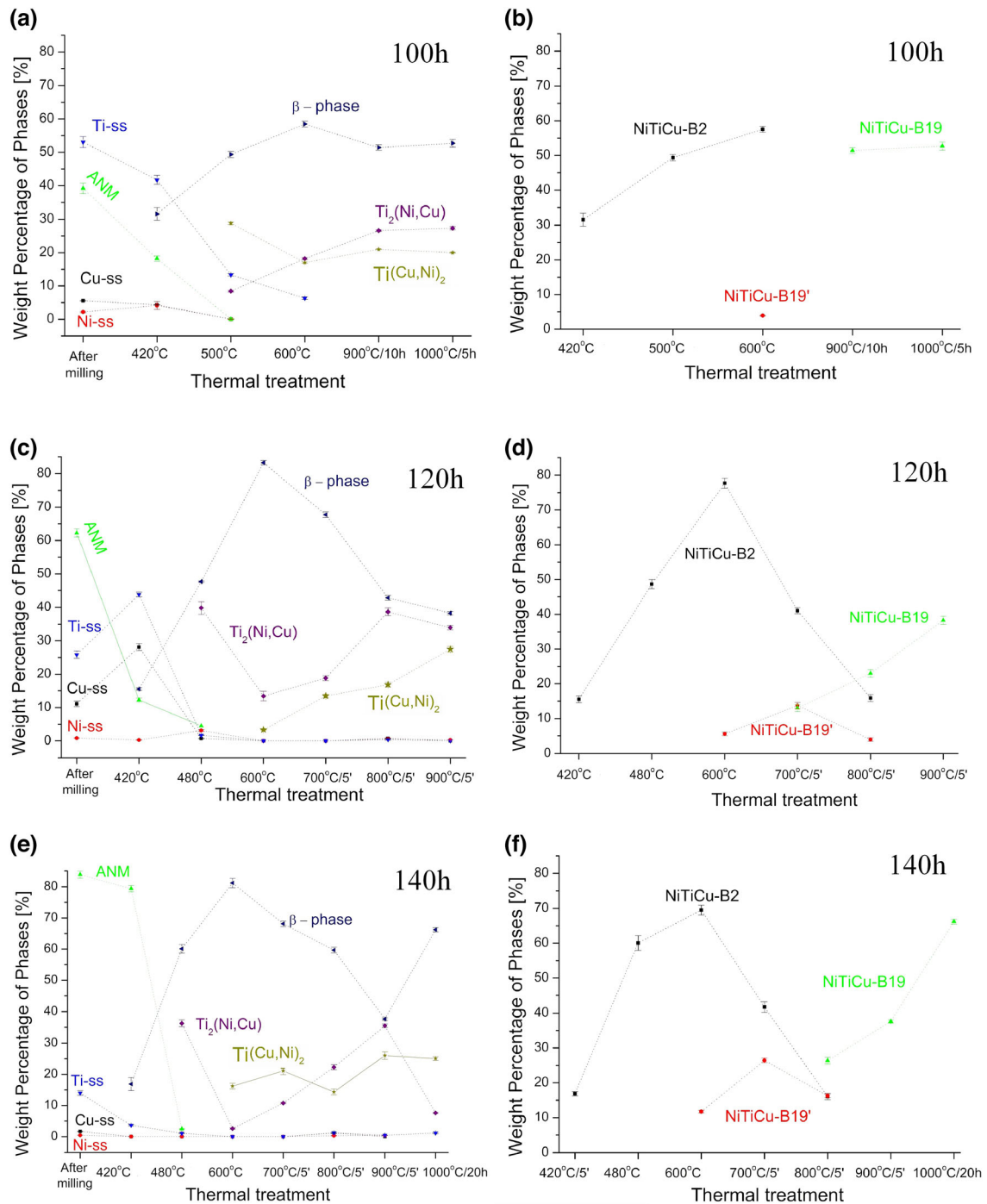


Fig. 5 The dependence of the percentage of phase shares on the heat treatment conditions for the phases determined from the Rietveld analysis for milling times: **a** 100 h, **b** 120 h, **c** 140 h, and the quantitative distribution of the β phase into phases resulting from MT present in RT **b** 100 h, **d** 120 h, and **f** 140 h. (where: ANM—

amorphous-nanocrystalline mixture, Ti-ss—titanium base solid solution, Ni-ss—nickel-based solid solution, Cu-ss—copper-based solid solution, NiTiCu-B2—parent phase with the B2 structure in NiTiCu alloy, NiTiCu-B19—orthorhombic martensite in NiTiCu alloy, NiTiCu-B19'—monoclinic martensite in NiTiCu alloy)

(Fig. 7a, b). Taking both these facts into account, it is clear that the small average size of the crystallites still limited triggering the MT.

The calculated diffractograms of the powders heated to 600 °C (temperature above the end of crystallization temperature— T_{P3E}) did not reveal the amorphous-crystalline mixture. In the alloy there were only the crystallized

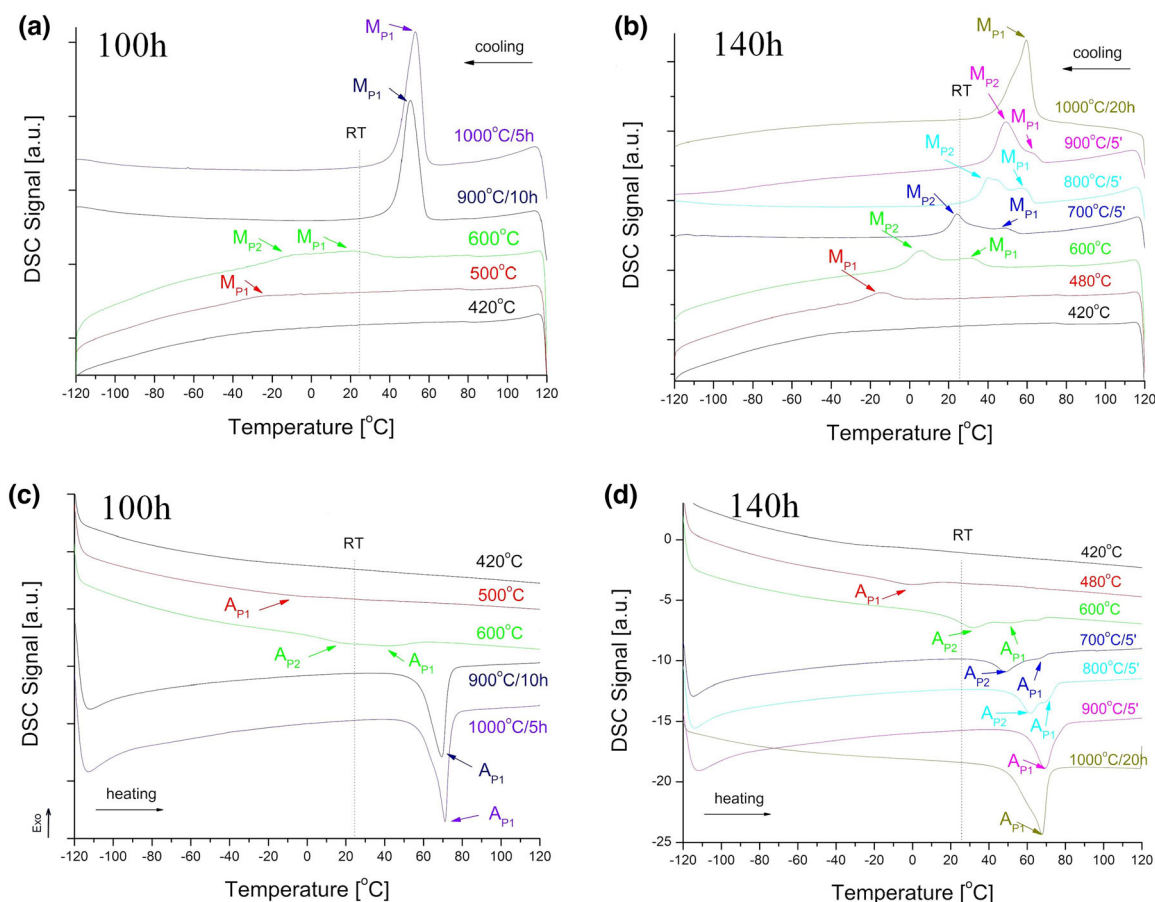


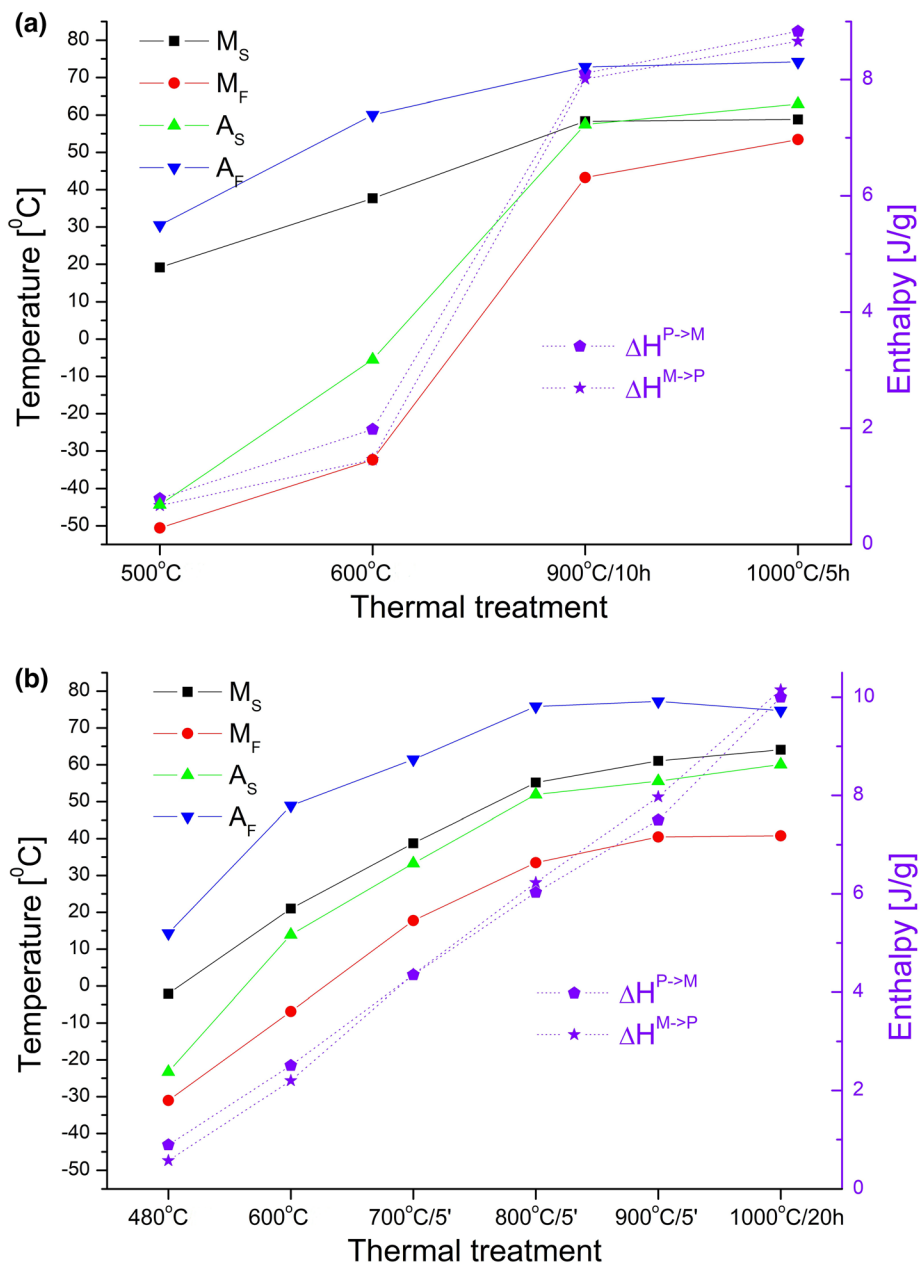
Fig. 6 DSC cooling/heating curves measured for powders milled 100 h (a) and 140 h (b) after various thermal treatment (Mp—peak temperature related to the forward martensitic transformation, Ap—peak temperature related to the reverse martensitic transformation)

phases—mainly the transformable β phase. Its share for the 100 h milled alloy was about 60%, and for the longer grinding times—83% (120 h) and 81% (140 h). Irrespective of the grinding time, in the RT diffractograms this phase consisted of areas formed with the B2-type structure and a small amount of the B19' monoclinic martensite (Fig. 5b, d, f). In addition to the β phase presence, the previously identified non-transformable phases of $\text{Ti}_2(\text{Ni,Cu})$ and $\text{Ti}(\text{Cu,Ni})_2$ crystallized. Figure 2 shows that the temperature region between T_{T2} and T_{T3} included fragments of Peak 2_1 and the entire Peak 3. Combining these facts with the quantitative phase analysis, it can be concluded that the transformation associated to Peak 3 was responsible for the crystallization and formation of the tetragonal $\text{Ti}(\text{Cu,Ni})_2$ phase. In addition, the presence of milled powders at temperatures from RT to T_{T3E} reduced the density of structural defects, associated with the relaxation of stresses accumulated during ball-powder collisions. The authors of works [34, 35] showed that in the NiTi alloy subjected to repeated cold rolling or mechanical alloying such a process began already in the range of 100–180 °C. All these factors influenced the reversible

martensitic transformation. First of all, there were two thermal peaks on the thermograms, both on the heating and cooling curves (Fig. 6—the green line). Secondly, the characteristic temperatures of the martensitic transformation increased by about 20–25 degrees. Thirdly, the enthalpy change (calculated as the sum of both thermal peaks M_{P1} and M_{P2} as well as A_{P1} and A_{P2}) increased to 1.8 J/g (100 h) and 2.3 J/g (140 h) (Fig. 7). Fourthly, the temperature ranges calculated as $M_{P1}-A_{P1}$ and $M_{P2}-A_{P2}$ were comparable and equaled 25° and 23°, respectively. In addition, the phase analysis showed that at RT, there was mainly the B2 parent phase and a small amount of the B19' monoclinic martensite. According to [33], these facts indicated that the copper share in the β phase increased to about 10–12at.%. However, the two-stage martensitic transformation proved that two areas of the β phase differed in the copper content by about 2–3%at. On the other hand, the martensitic transformation sequence remained the one-stage B2 \leftrightarrow B19'.

Summing up these results, the energy supplied by increasing the temperature was insufficient for the alloy with the nominal chemical composition of $\text{Ni}_{25}\text{Ti}_{50}\text{Cu}_{25}$

Fig. 7 Characteristic parameters of the MT determined for powder milled 100 h (a) and 140 h (b) after various thermal treatment



(weight 20 g) to undergo the single-step martensitic transformation to the orthorhombic martensite. Additional heat treatments at elevated temperatures and/or extended times were necessary for crystallized alloys.

Influence of Annealing on the Structure and Course of Martensitic Transformation in Crystallized Alloys

The martensitic transformation course improved notably with an additional heat treatment. In the case of the 100 h milled alloy, the annealing temperature was raised to 900 °C and 1000 °C, and the annealing time was extended

to 10 h and 5 h, respectively. The analysis of the quantitative weight percentage of the produced phases showed an increase in the transformable β phase share to 51% (900 °C/10 h) and 52% (1000 °C/5 h) (Fig. 5a). The $Ti_2(Ni,Cu)$ and $Ti(Cu,Ni)_2$ equilibrium phases shares: also grew after crystallization. At the applied annealing temperatures, the alloy was subjected to the rules of phase equilibrium systems and underwent the partial decomposition of the β phase. According to the measured diffraction patterns, this phase took on the structure of orthorhombic martensite B19 at RT (Fig. 5b). The transformation hysteresis, measured as the difference between the temperatures M_P and A_P , was relatively narrow and equaled 16°

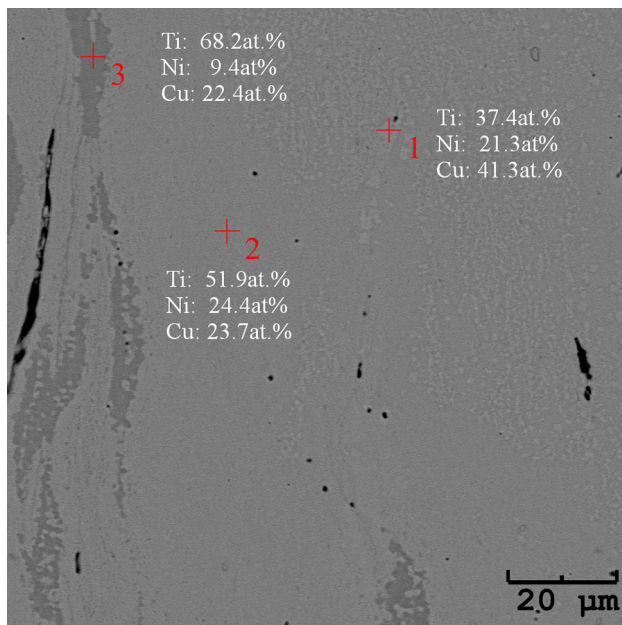


Fig. 8 SEM image with results of EDS analysis measured for the cross-section of alloy milled 140 h and aged at 800 °C for 5 min

(900 °C/10 h) and 17° (1000 °C/5 h). It is a characteristic parameter of the B2 ↔ B19 transformation, reported in the literature for NiTiCu alloys containing 25%at. of Cu [33]. Compared to the state after crystallization, the annealing conditions positively affected the chemical composition homogenization, which narrowed the transformation range calculated as a difference between M_s and M_f as well as A_s and A_f . In addition, the transformation enthalpy increased to over 8 J/g (Fig. 7a). This value was higher than the one obtained by the authors of [36] for melt-spinning strips of the Ni₂₅Ti₅₀Cu₂₅ alloy.

The alloy milled for 120 h and 140 h, in the temperature range of 700–900 °C and then annealed for a relatively short time of 5 min showed the increased share of non-transformable phases Ti₂(Ni,Cu) and Ti(Cu,Ni)₂, as previously described. This phenomenon took place due to the β phase decomposition under the equilibrium conditions, which was visible in the SEM image (Fig. 8). The grayscale areas corresponding to Point 1 refer to the Ti(Cu,Ni)₂ phase, Point 2—to the B19 orthorhombic martensite, and Point 3—to the Ti₂(Ni,Cu) phase. The Ti₂(Ni,Cu) phase had a crystallographic structure of the Ti₂Ni phase, where nickel atoms were replaced by copper, constituting a total amount of 33%at. On the other hand, the Ti(Cu,Ni)₂ phase fit perfectly in the area of the TiCu₂ occurrence, which was found in the cross-section of the ternary Ti–Ni–Cu phase diagram at 800 °C and 870 °C [34]. The Ti(Cu,Ni)₂ possessed a crystallographic structure of the MoSi₂ phase (tetragonal I4/mmm), where titanium atoms (with a larger

atomic radius of 2.48 Å [35]) occupied the Mo position, while nickel and copper atoms with smaller atomic radii (1.93 Å and 1.86 Å [35]), occupied positions intended for Si [37]. These results confirmed the models of crystallographic structures previously adopted for the Rietveld's analysis.

The DSC curves courses and the martensitic transformation behavior for the alloys milled for 120 h and 140 h were very similar. Due to the alloy's better homogenization after the extended grinding time, only the results for the 140 h ground alloy are described. The evolution of the martensitic transformation for this alloy is shown in Figs. 6b and d. Annealing at 600 °C and 700 °C, i.e., above crystallization point, changed the course of the martensitic transformation to a two-stage one. However, it was a one-step transformation with the B2 ↔ B19' sequence (only the B19' martensite was present Fig. 5f) occurring in the areas slightly differing in chemical composition. Moreover, annealing at 700 °C for 5 min increased the characteristic temperatures of the MT by about 20 degrees. It proved a significant enrichment of the β-phase in copper [33].

Similarly, annealing at 800 °C and 900 °C for 5 min caused the shift of the phase transitions into higher temperatures characteristic for the B2 ↔ B19 transformation. In addition, the temperature transition ranges (M_f – M_s and A_f – A_s) narrowed to about 20°. For the alloy annealed at 800 °C, the difference between the M_{P1} and A_{P1} temperatures was reduced to 13°. According to the results published in [33], this transformation referred to the B2 ↔ B19 sequence. The difference between M_{P2} and A_{P2} was still about 20°, which was characteristic for the transformation with the monoclinic martensite B19'. It confirmed the two areas which differed in chemical composition: one strictly corresponding to the nominal composition, and the other—with the copper addition of about 14–19%at.

Increasing the annealing temperature to 900 °C (for 5 min) caused the further β phase decomposition into the equilibrium phases: Ti₂(Ni,Cu) and Ti(Cu,Ni)₂ which did not participate in the martensitic transformation. Decomposition decreased the β phase weight fraction at the expense of the higher shares of both non-transformable phases (Fig. 5e). The β phase, at room temperature, ultimately assumed the structure of the B19 orthorhombic martensite. The DSC cooling curves (Fig. 6b—the magenta line) showed two additional stages of the B19 martensite. Contrary to that, the reversible transformation occurred in one stage (Fig. 6d—the magenta line). In order to intensify the alloying elements diffusion, the alloy milled at 140 h was sintered at 1000 °C for 20 h. In consequence, the B2 ↔ B19 transformation sequence was obtained at the temperatures expected for the nominal chemical composition. Additionally, the transformation enthalpy increased to

over 10 J/g (Fig. 7b). This was the result of an intensive increase in the β phase share at the expense of the lowered amount of $\text{Ti}_2(\text{Ni,Cu})$ (Fig. 5e, f).

Summary

The alloy with a nominal chemical composition of $\text{Ni}_{25}\text{Ti}_{50}\text{Cu}_{25}$, characterized by a onestage reversible martensitic transformation with the B2 \leftrightarrow B19 sequence was produced via high-energy ball milling. However, after milling for 100–140 h, the alloys consisted of an amorphous-nanocrystalline mixture. The temperature high enough for the partial crystallization did not provide sufficient structural, chemical, and phase conditions for the reversible martensitic transformation. Hence, the crystallization proceeded in the three distinguishable stages. The first one was related to the crystallization of solid solutions based on the alloying elements. The weight percentages analysis of the forming phases indicated the crystallization of the transformable β phase in the whole temperature range from 361 to 556 °C. However, its most intense part was related to the thermodynamic conditions provided in the second stage when the equilibrium $\text{Ti}_2(\text{Ni,Cu})$ phase formed. In the last crystallization stage the second equilibrium phase $(\text{Cu,Ni})_2\text{Ti}$ occurred.

The highest weight percentages of the transformable phase β were obtained in the alloys milled for 120 h and 140 h after their thermal treatment at 600 °C for 5 min. Although the over 80% weight share belonged to the parent phase B2, its small part underwent the martensitic transformation. The short period of the elevated temperature did not provide sufficient structural conditions to trigger the martensitic transformation. The relatively small average crystallite size of about 6 nm suppressed the martensitic transformation. A beneficial procedure was to extend the grinding time to 140 h, increasing sintering temperature to 1000 °C for several hours. Such conditions ensured the proper homogenization of the alloy and the increased share of the β phase. Moreover, the alloy in the powder form showed the presence of the bulk-like reversible martensitic transformation with a relatively high enthalpy of 10 J/g.

Open Access This article is licensed under a Creative Commons Attribution 4.0 International License, which permits use, sharing, adaptation, distribution and reproduction in any medium or format, as long as you give appropriate credit to the original author(s) and the source, provide a link to the Creative Commons licence, and indicate if changes were made. The images or other third party material in this article are included in the article's Creative Commons licence, unless indicated otherwise in a credit line to the material. If material is not included in the article's Creative Commons licence and your intended use is not permitted by statutory regulation or exceeds the permitted use, you will need to obtain permission directly from the copyright

holder. To view a copy of this licence, visit <http://creativecommons.org/licenses/by/4.0/>.

Data Availability The data presented in this study are available on request from the corresponding authors.

References

- Mineta T, Kasai K, Sasaki Y, Makino E, Kawashima T, Shibata T (2009) Flash-evaporated TiNiCu thick film for shape memory alloy micro actuator. *Microelectron Eng* 86(4–6):1274–1277
- Miller DA, Dimitris CL (2000) Thermomechanical characterization of NiTiCu and NiTi SMA actuators: influence of plastic strain. *Smart Mater Struct* 9:640–652
- Saikrishna CN, Ramaiah KV, Bhaumik SK (2006) Effects of thermo-mechanical cycling on the strain response of Ni–Ti–Cu shape memory alloy wire actuator. *Mater Sci Eng A* 428:217–224
- Tsoi KA, Schrooten J, Stalmans R (2004) Part I. Thermomechanical characteristics of shape memory alloys. *Mater Sci Eng A* 368:286–298
- Funakubo H (1984) Shape memory alloys. Gordon and Breach, London
- Pelton AR, Russell SM, DiCello J (2003) The physical metallurgy of nitinol for medical applications. *JOM* 55:33–37
- Frenzel J, Zhang Z, Neuking K, Eggeler G (2004) High quality vacuum induction melting of small quantities of NiTi shape memory alloys in graphite crucibles. *J Alloys Com* 28:214–223
- Tsai D-C, Chiang C-H (2015) Vacuum arc melting processes for biomedical Ni-Ti shape memory alloys. *MATEC Web Conf* 30:01004
- Qadir R, Mohammed S, K ok M, Qader I (2021) A review on NiTiCu shape memory alloys: manufacturing and characterizations. *J Phys Chem Funct Mater* 4(2):49–56
- Goryczka T, Ochinn P (2006) Microstructure, texture and shape memory effect in $\text{Ni}_{25}\text{Ti}_{50}\text{Cu}_{25}$ ribbons and strips. *Mat Sci Eng A* 438–440:714–718
- Goryczka T (2013) $\text{Ni}_{25}\text{Ti}_{50}\text{Cu}_{25}$ shape memory alloy produced by nonconventional techniques. In: Braz Fernandes FM (ed) *Shape Memory Alloys—Processing, Characterization and Applications*. Rijeka, InTech, pp 53–76
- Fu Y, Du H (2003) RF magnetron sputtered TiNiCu shape memory alloy thin film. *Mater Sci Eng A* 339:10–16
- Craciunescu C, Hamdy AS (2013) The effect of copper alloying element on the corrosion characteristics of Ti-Ni and ternary Ni-Ti-Cu meltspun shape memory alloy ribbons in 0.9% NaCl solution. *Int J Electrochem Sci* 8:10320–10334
- Elahinia M, Moghaddam NS, Andani MT, Amerinatanzi A, Bimber BA, Hamilton RF (2016) Fabrication of NiTi through additive manufacturing: a review. *Prog Mater Sci* 83:630–663
- Shahmir H, Nili-Ahmadabadi M, Huang Y, Jung JM, Kim HS, Langdon TG (2015) Shape memory effect in nanocrystalline NiTi alloy processed by high-pressure torsion. *Mater Sci Eng A* 626:203–206
- Hu L, Jiang S, Zhang Y (2017) Role of severe plastic deformation in suppressing formation of R phase and Ni_4Ti_3 precipitate of NiTi shape memory alloy. *Metals*. <https://doi.org/10.3390/met7040145>
- Craciunescu CM, Silva RJC, Fernandes FMB (2015) Fracture modes during severe plastic deformation of NiTi shape memory alloys. *Phys Metals Metallogr* 116:698–705
- Tang M, Zhang Y, Jiang S, Yu J, Yan B, Zhao C, Yan B (2020) Microstructural evolution and related mechanisms in NiTiCu shape memory alloy subjected local canning compression. *Internet* 118:106700

19. Tomochika H, Kikuchi H, Araki T, Nishida M (2003) Fabrication of NiTi intermetallic compound by a reactive gas laser atomization process. *Mater Sci Eng A* 356:122–129
20. Wang J-W, He D-Y, Wu X, Guo X-Y, Tan Z, Zhou Z, Shao W (2022) Characterization of pre-alloyed NiTi powders produced by electrode induction-melting inert gas atomization for additive manufacturing. *J Min Metall Sect B-Metall* 58(2):219–228
21. Makifuchi Y, Terunuma Y, Nagumo M (1997) Structural relaxation in amorphous Ni-Ti alloys prepared by mechanical alloying. *Mater Sci Eng A* 226–228:12–316
22. Tian B, Tong YX, Chen F, Liua Y, Zheng YF (2009) Phase transformation of NiTi shape memory alloy powders prepared by ball milling. *J Alloys Compd* 477:576–579
23. Salwa P, Goryczka T (2021) Influence of batch mass on formation of NiTi shape memory alloy produced by high-energy ball milling. *Metals* 11:1908
24. Salwa P, Goryczka T (2020) Crystallization of mechanically alloyed Ni₅₀Ti₅₀ and Ti₅₀Ni₂₅Cu₂₅ shape memory alloys. *J Mater Eng Perform* 29:2848–2852
25. Goryczka T, Salwa P, Zubko M (2021) High-energy ball milling conditions in formation of NiTiCu shape memory alloys. *Microsc Microanal* 28(3):939–945
26. TA Instruments Deconvolution of Thermal Analysis Data using Commonly Cited Mathematical Models. TA431. www.tainstruments.com. Accessed 20 Jan 2023
27. Hill RJ, Howard CJ (1987) Quantitative phase analysis from neutron powder diffraction data using the Rietveld method. *J App Crystall* 20(6):467–474
28. Peterlechner M, Bokeloh J, Wilde G, Waitz T (2010) Study of relaxation and crystallization kinetics of NiTi made amorphous by repeated cold rolling. *Acta Mater* 58:6637–6648
29. Louzguine DV, Inoue A (2000) Crystallization behavior of Ti₅₀Ni₂₅Cu₂₅ amorphous alloy. *J Mater Sci* 35:4159–4164
30. Liu Y, Xie ZL, Tong YX, Lim CW (2006) Properties of rapidly annealed Ti₅₀Ni₂₅Cu₂₅ melt-spun ribbon. *J Alloys Compd* 416:188–193
31. Wang CP, Liu XJ, Jiang M, Ohnuma I, Kainuma R, Ishida K (2005) Thermodynamic database of the phase diagrams in copper base alloy systems. *J Phys Chem Solids* 66(2–4):256–260
32. Tang W, Sandstrom R, Miyazaki S (2000) Phase equilibria in the pseudobinary Ti_{0.5}Ni_{0.5}-Ti_{0.5}Cu_{0.5} system. *J Phase Eq* 21(3):227–234
33. Moberly WJ, Melton KN (1990) Ni-Ti-Cu shape memory alloys. In: Duerig TW, Melton KN, Stöckel D, Wayman CM (eds) *Engineering aspects of shape memory alloys*. Butterworth-Heinemann Ltd, London, pp 46–57
34. Van Loo FJJ, Bastin GF, Leenen AJH (1978) Phase relations in the ternary Ti-Ni-Cu system at 800 and 870°C. *J Less-Common Met* 57:111–121
35. Ghosh DC, Biswas R (2002) Theoretical calculation of absolute radii of atoms and ions. Part 1. The atomic radii. *Int J Mol Sci* 3:87–113
36. Chang SH, Wu SK, Kimura H (2007) Annealing effects on the crystallization and shape memory effect of Ti₅₀Ni₂₅Cu₂₅ melt-spun ribbons. *Intermetallics* 15:233–240
37. Salamon M, Strohm A, Voss T, Laitinen P, Riihimäki I, Divinski S, Frank W, Raisanen J, Mehrer H (2004) Self-diffusion of silicon in molybdenum disilicide. *Phil Mag* 84:737–756

Publisher's Note Springer Nature remains neutral with regard to jurisdictional claims in published maps and institutional affiliations.